The Company of Biologists

RESEARCH ARTICLE

A dual phenotype of MDA-MB-468 cancer cells reveals mutual regulation of tensin3 and adhesion plasticity

Astrid Veß[1,¶], Ulrich Blache[1,*,¶], Laura Leitner[1,2], Angela R. M. Kurz[1,2,§], Anja Ehrenpfordt[1], Michael Sixt[3] and Guido Posern[1,2,**]

ABSTRACT

A change regarding the extent of adhesion – hereafter referred to as adhesion plasticity – between adhesive and less-adhesive states of mammalian cells is important for their behavior. To investigate adhesion plasticity, we have selected a stable isogenic subpopulation of human MDA-MB-468 breast carcinoma cells growing in suspension. These suspension cells are unable to re-adhere to various matrices or to contract three-dimensional collagen lattices. By using transcriptome analysis, we identified the focal adhesion protein tensin3 (Tns3) as a determinant of adhesion plasticity. Tns3 is strongly reduced at mRNA and protein levels in suspension cells. Furthermore, by transiently challenging breast cancer cells to grow under non-adherent conditions markedly reduces Tns3 protein expression, which is regained upon re-adhesion. Stable knockdown of Tns3 in parental MDA-MB-468 cells results in defective adhesion, spreading and migration. Tns3-knockdown cells display impaired structure and dynamics of focal adhesion complexes as determined by immunostaining. Restoration of Tns3 protein expression in suspension cells partially rescues adhesion and focal contact composition. Our work identifies Tns3 as a crucial focal adhesion component regulated by, and functionally contributing to, the switch between adhesive and non-adhesive states in MDA-MB-468 cancer cells.

KEY WORDS: Cell−matrix adhesion, Tensin3, Breast cancer, Actin, Migration

INTRODUCTION

Changing the adhesive properties of cells is important for many biological processes. These include early steps in development like primordial germ cell migration but also processes in adult organisms, such as leukocyte extravasation, dendritic cell homing, neuroregeneration by glia cells and metastasis of tumor cells (Paluch et al., 2016). In cancer, breakout of cells from solid tumors requires increased motility and reduced cell adhesion. Following their systemic spread via the circulation, the opposite is necessary for the colonization of distal organs, which depends on a (partial) reversion into less motile cells with regained matrix adhesion (Gunasinghe et al., 2012; Chaffer et al., 2016). However, little is known about the cellular regulation of the underlying adhesion plasticity.

Cell−matrix adhesions are macromolecular structures that link the intracellular cytoskeleton to the extracellular matrix (ECM) and are involved in cell attachment, spreading and migration. These adhesion contacts contain the transmembrane integrins, which connect the ECM to the intracellular actin cytoskeleton via adapter proteins (Sun et al., 2016). It is evident that the precise molecular composition of these integrin-based adhesion complexes is critical for their function. Depending on the cell type, the so-called 'integrin adhesome' can vary a lot and several hundreds of proteins contribute to the adhesome, as revealed by proteomic analyses (Humphries and Reynolds, 2009; Schiller et al., 2011; Horton et al., 2015). On the basis of function, composition and appearance cell−matrix adhesions can be classified (Sun et al., 2016). Focal adhesions are mainly located near the cell periphery since they establish early cell−matrix contacts. They are complex assemblies of many different proteins including the characteristic adapters vinculin, talin, paxillin, and the tyrosine-phosphorylated proteins p130Cas, FAK and Src (Zamir and Geiger, 2001). In contrast, the fibrillar adhesions of fibroblasts (previously termed ECM contacts) are found not just at the cell periphery but throughout the entire cell (Geiger and Yamada, 2011; Sun et al., 2016). These fibrillar adhesions are elongated structures that are associated with mature ECM fibrils and are considered to be late cell−matrix adhesions. Key components of fibrillar adhesions are extracellular fibronectin, the fibronectin receptor $\alpha5\beta1$ integrin and members of the tensin protein family (Zamir et al., 1999, 2000; Geiger et al., 2001).

Vertebrate tensins represent a family of large cytoskeletal proteins (~180 kDa) encoded by four genes (*Tns1*, *Tns2*, *Tns3*, *Tns4*) (Lo, 2004). Tns1-3 are focal contact proteins that, via their integrin-binding PTB domain at the C-terminus, link the cytoplasmic tails of β-integrins to the actin cytoskeleton bound by their N-terminal actin-binding domain (Calderwood et al., 2003). In doing so, Tns1-3 maintain the tension between in- and outside of a cell. A fourth gene, Cten (*Tns4*), encodes a much smaller protein lacking the actin-binding domain of the larger Tns isoforms (Lo, 2004; Haynie, 2014). It has previously been shown that *Tns3* is deregulated in cancer and has implications in cell migration, invasion and tumorigenesis, but its role remains controversial (Cui et al., 2004; Katz et al., 2007; Martuszewska et al., 2009; Qian et al., 2009; Cao et al., 2012; Shinchi et al., 2015).

Gaining deeper insights into the plasticity of cell-matrix adhesion is of utmost importance to better understand many biological processes, including metastasis. In this regard, we desired a cell culture model system reproducing an adhesive and a non-adhesive phenotype of breast cancer cells of the same genetic background. Therefore, we generated a non-adhesively growing (suspension)

[1]Institute for Physiological Chemistry, Medical Faculty, Martin Luther University Halle-Wittenberg, 06114 Halle (Saale), Germany. [2]Max Planck Institute of Biochemistry, 82152 Martinsried near Munich, Germany. [3]Institute of Science and Technology, 3400 Klosterneuburg, Austria.
*Present address: Laboratory for Orthopedic Biomechanics, ETH Zürich, 8091 Zürich , Switzerland. §Present address: Walter Brendel Center of Experimental Medicine, Ludwig-Maximilians-University, 81377 München, Germany.
¶These authors contributed equally to this work

**Author for correspondence (guido.posern@uk-halle.de)

G.P., 0000-0002-0400-0222

Journal of Cell Science

subclone of the MDA-MB-468 breast cancer cells. Here, we report on Tns3 being a main player and target during adhesion plasticity. Identified by transcriptome analysis, Tns3 is dramatically downregulated by loss of cell adhesion. Vice versa, knockdown of Tns3 impairs cell adhesion and migration by affecting focal contact composition and dynamics. Moreover, the ectopic expression of Tns3 after loss of cell adhesion (and loss of endogenous Tns3 expression) is able to partially restore cell-matrix adhesion and migration. Our results show that the expression as well as the function of Tns3 are tightly intertwined with the cell-matrix adhesion in MDA-MB-468 breast cancer cells.

RESULTS
Generation and characterization of MDA-MB-468 suspension cells

To gain insights into the plasticity of cell−matrix adhesion and its determinants, a cell culture model consisting of cells that only differ in their mode of adhesion would be a powerful tool. Towards this aim, we have established non-adhesively growing subpopulations of human breast cancer MDA-MB-468 cells. These MDA-MB-468 suspension subclones were selected by repeatedly collecting floating, non-adherent cells from standard MDA-MB-468 cultures and re-cultivating them again on tissue culture dishes. In doing so, a stable suspension subculture was established after 12−15 passages. We termed this isogenic suspension subculture 468^{susp}, while we refer to the adherent parental cell line as 468^{par}. The morphology of these two MDA-MB-468 subpopulations is different, as revealed by phase-contrast microscopy and F-actin staining (Fig. 1A). Whereas 468^{par} cells grow adherently and spread out on tissue culture dishes, 468^{susp} cells grow in suspension and tend to form grape-like cell clusters. Moreover, our adhesion-independent 468^{susp} cell line does not change the suspension growth mode even when provided with adhesive substrates, such as type I collagen, fibronectin or matrigel (Fig. 1B, and data not shown). Of note, the rate of proliferation and cell death (apoptosis) was found to be fairly similar between both subpopulations, suggesting independence from anoikis induction (Fig. 1C,D).

Since 468^{susp} cells did not form cell−matrix contacts on flat 2D substrates, we examined whether these cells also display impaired adhesion and force transmission within 3D environments. To address this point, we performed a collagen contraction assay. Three independently isolated MDA-MB-468 subclones were encapsulated in 3D collagen hydrogels and the cell-mediated contraction was evaluated after four days. 468^{susp} cells lacked the ability to contract collagen gels independently of the cell concentration (Fig. 1E). In contrast, 468^{par} cells contracted the collagen hydrogels to more than 20% as a function of cell concentration, similar to other adhesively growing cell lines (data not shown). These results show impaired force transmission between the ECM and the actin cytoskeleton in 468^{susp}, and also indicate defective cell−matrix interactions in a 3D environment.

The main cell−matrix receptors are integrin heterodimers exposed on the cell surface. Hence, we analyzed by flow cytometry whether the surface expression of different integrin subunits in 468^{par} and 468^{susp} cells is altered. Only integrin α6, β4 and β1 displayed a significant change in surface expression (Fig. 1F). Whereas integrin α6 and β4 was increased, expression of integrin β1 was decreased in 468^{susp} cells compared to 468^{par} cells. Most integrins, however, were either not expressed (α1, α4, β2; data not shown) or showed no significant difference (α2, α5, αV, β2). Hence, our data indicate that 468^{susp} cells are not defective for integrin presentation but slightly change the subclasses on their cell surface.

A key coordinator in cell adhesion is the small GTPase Rac. It reorganizes the actin cytoskeleton and, therefore, controls cell behavior including adhesion, spreading and migration. To determine potential differences between parental and suspension cells, the amount and activity of Rac1 protein was determined. Rac1 was significantly less active in 468^{susp} cells compared to the 468^{par} cells, as revealed by a PAK-CRIB pull-down assay (Fig. 1G). However, immunoblotting of total lysates showed that Rac1 whole protein amounts were comparable.

Loss of Tns3 in MDA-MB-468 upon loss of adhesion

To investigate the underlying differences between 468^{par} and 468^{susp} cells without bias, a genome-wide transcriptome profiling was performed. For this purpose, RNA of 468^{par} cells (three independent RNA preparations) and of 468^{susp} cells (RNA preparations of three independently isolated subpopulations; 468^{susp} A, 468^{susp} B, 468^{susp} C) were used for affymetrix microarray analysis. By using a false discovery rate of <5%, we identified >300 genes that were significantly up- or downregulated (at least two-fold) in the parental versus suspension cell lines (Table S1). Of all genes downregulated in the suspension cells, *Tns3* showed the strongest effect, with an average reduction of signal intensity of more than nine-fold in the microarray analysis (Fig. 2A). Tns3 is an adapter protein that connects the cytoplasmic tail of integrins to the actin cytoskeleton (Calderwood et al., 2003; Lo, 2004). To this end, we thus decided to further analyse the role of Tns3 in adhesion plasticity.

Differential expression of Tns3 in 468^{susp} cells compared to 468^{par} cells was validated by quantitative reverse transcription (qRT)-PCR, which showed a six-fold decrease of *Tns3* mRNA levels in 468^{susp} cells (Fig. 2B). However, Tns3 protein was almost undetectable by immunoblotting in 468^{susp} cells (Fig. 2C). Quantification revealed a 30-fold downregulation in the suspension cells (Fig. 2D). In comparison, the transcript and protein levels of other Tns family members were also analyzed by qRT-PCR and western blot analysis. The transcript levels of *Tns2* were down, whereas amounts of *Tns1* and *Tns4* mRNA were increased in 468^{susp} cells (Fig. S1A). However, the protein levels of Tns1 and Tns2 were unaffected, whereas that of Tns4 was increased in 468^{susp} cells (Fig. 2E). We further investigated whether expression levels of other major focal adhesion adapter proteins are also affected in 468^{susp} cells. Interestingly, we observed no decrease on protein or transcript levels of other focal adhesion proteins like vinculin, FAK or talin (Fig. 2F, Fig. S1B,C). However, immunofluorescence staining revealed that these proteins do not localize to focal-adhesion-like structures in 468^{susp} cells, consistent with their lack of focal adhesions (data not shown).

To elucidate whether loss of cell−matrix adhesion is sufficient to induce downregulation of Tns3 in 468^{par} cells, these cells were cultivated on non-adhesive polyHEMA-coated substrates for up to 72 h (Fig. 3). However, unlike the stably selected 468^{susp} cells, these cells restored matrix adhesion after non-adhesive growth when transferred back to tissue culture plastic (Fig. 3A). In this experiment we were able to show that transient loss of adhesion resulted in a significant decrease of Tns3 in MDA-MB-468 (Fig. 3B,C). Within the first 24 h Tns3 transcript and protein levels dropped to around 60% and reached <40% of their original expression after 72 h. Importantly, re-adhesion of MDA-MB-468 cells restored Tns3 at both protein and mRNA levels to almost 100% within 24 h. Similar results were obtained with MCF7 breast cancer cells (Fig. S2). However, in MCF7 cells the dynamics were slightly different, as levels of Tns3 decreased more and were just partially
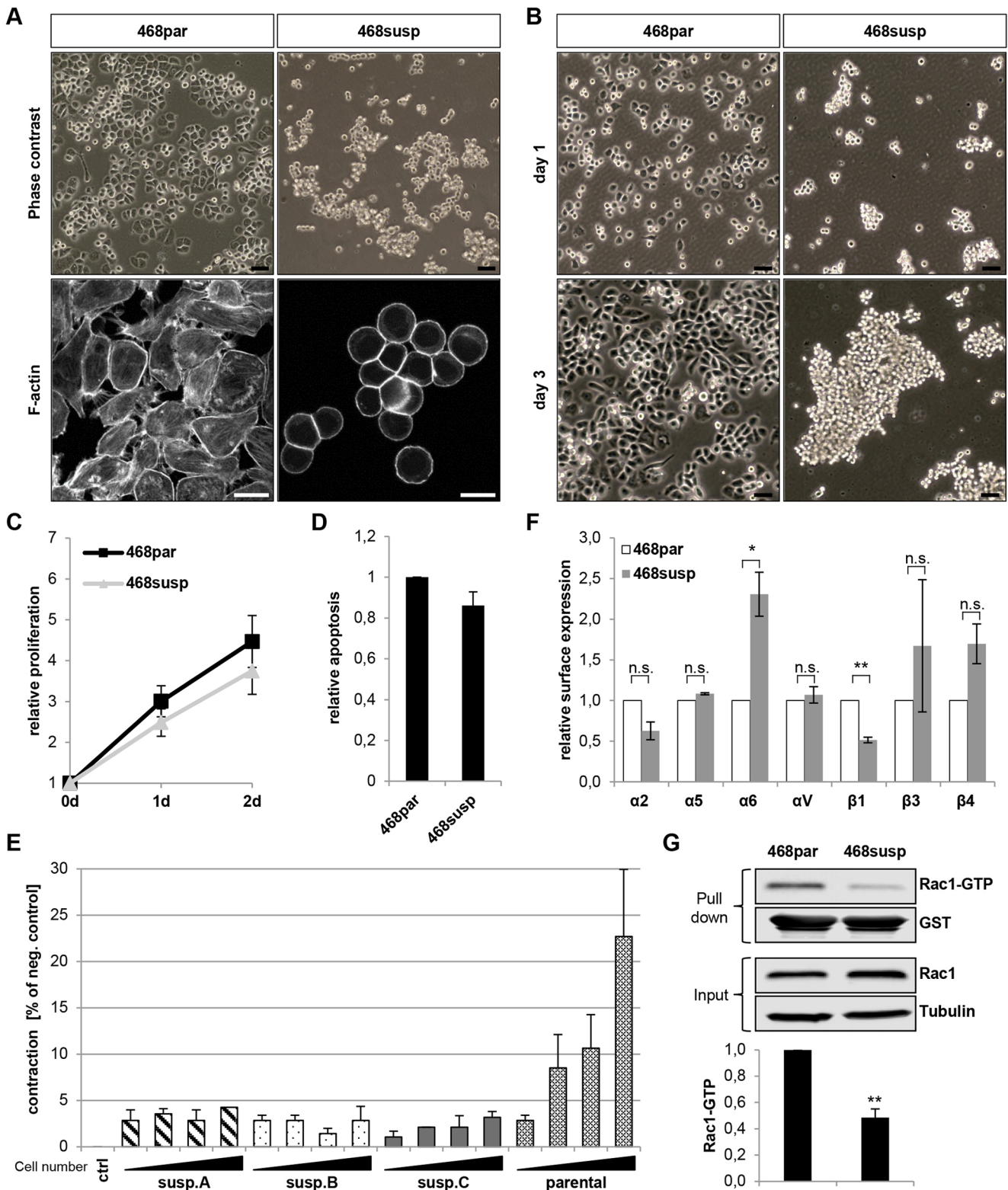
Fig. 1. Characterization of MDA-MB-468 subclones selected for non-adhesive growth. (A) Representative phase-contrast images and F-actin cytoskeleton staining (phalloidin) of parental and suspension MDA-MB-468 breast cancer cells. Scale bars: 50 µm (phase contrast), 10 µm (F-actin staining). (B) Phase-contrast images of indicated cells cultured on collagen-coated substrates for indicated time periods. Scale bars: 50 µm. (C) Proliferation rate measured in 468^{par} and 468^{susp} cells in a colorimetric assay (n=3). (D) Apoptosis rate in 468^{par} and 468^{susp} cells by measuring caspase-3 activity (n=3). (E) Collagen contraction assay. Increasing cell numbers of the indicated cell lines were mixed with collagen in medium containing EGF, and allowed to solidify in 96-well plates. The area of the collagen lattices was measured after 4 days. Shown is the shrinkage of the collagen gel diameter of cell-free negative control in percent (n=3). (F) Flow cytometry analysis of integrin surface levels (n=4). (G) GST pulldown of Rac1-GTP. Precipitated proteins (GST pulldown) and total lysates (input) were immunoblotted with the indicated antibodies. Quantification of bound active Rac1 normalized to input Rac1 (n=5). All error bars represent ±s.e.m. P-values were calculated using an unpaired one-sample Student's t-test (*P≤0.05, **P≤0.01).
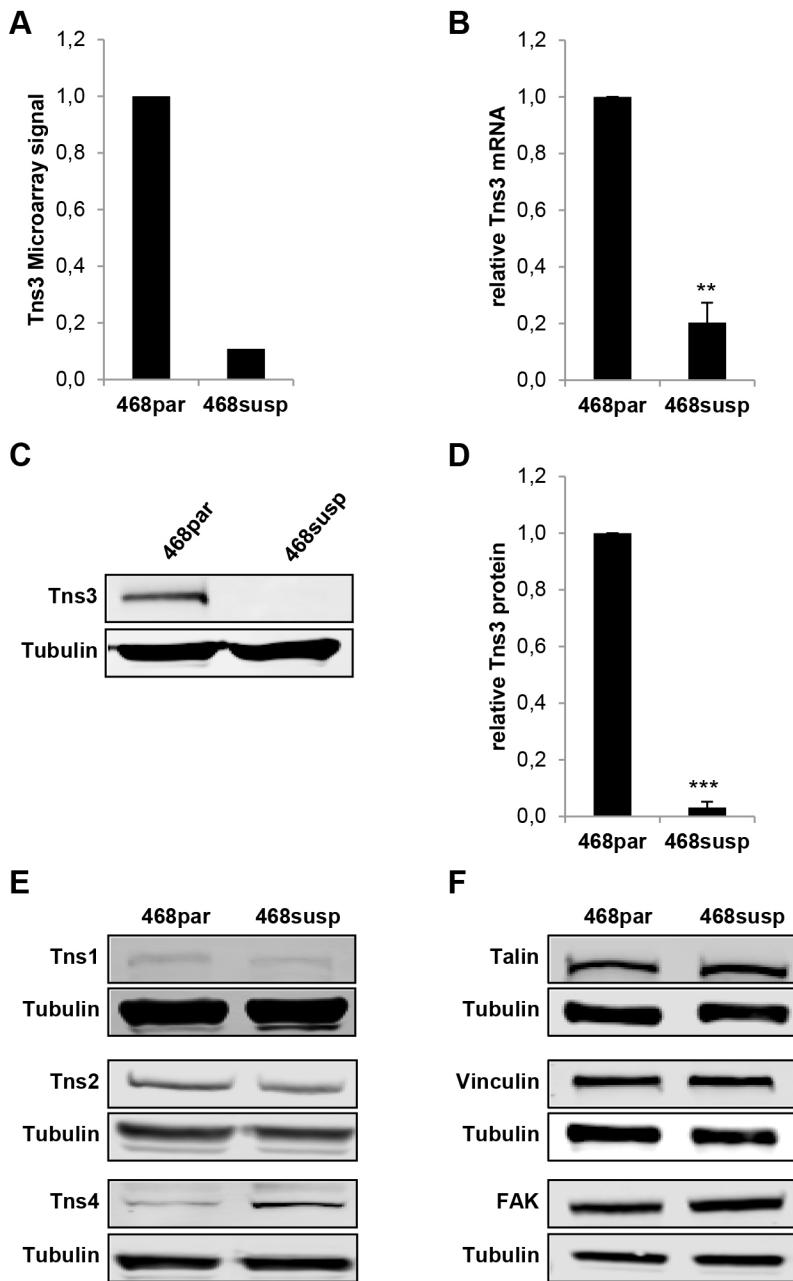
Fig. 2. Tns3 expression is decreased in stable suspension subclones. (A) Relative microarray signal intensity for *Tns3* in MDA-MB-468par and -468susp cells. Shown is the average of three independent experiments. (B) *Tns3* mRNA transcript levels were determined by qRT-PCR, normalized to ALAS1 and HPRT1 in 468par and 468susp cells. (C) Western blot of Tns3 in total cell lysates from indicated cells. Tubulin was used as loading control. (D) Quantification of Tns3 protein levels normalized to tubulin. (E) Representative western blot of Tns1, Tns2 and Tns4 in total cell lysates from indicated cells. Tubulin was used as a loading control. (F) Representative western blot of talin, vinculin and FAK in total cell lysates from indicated cells. Tubulin was used as a loading control. All error bars represent ±s.e.m., $n \geq 3$. All P-values were calculated using an unpaired one-sample Student's *t*-test (**$P \leq 0.01$, ***$P \leq 0.001$).

restored within 48 h of re-adhesion. In contrast to Tns3, protein levels of talin and vinculin were not significantly altered by cultivating MDA-MB-468par or MCF7 cells on non-adhesive polyHEMA substrate (Fig. 3D,E and Fig. S2D,E).

Tns3-knockdown influences adhesion and migration capacity of 468par cells

To address whether loss of Tns3 alone interferes with cell–matrix adhesion of MDA-MB-468 cells, stable knockdown of Tns3 in 468par cells was performed. Therefore, 468par cells were lentivirally transduced with three independent constructs encoding *Tns3*-specific shRNAs or a control shRNA. Expression of *Tns3*-specific shRNAs resulted in up to 80% decreased Tns3 levels (Fig. 4A,B). To gain further insights into the defects of 468par cells lacking Tns3 we performed cell adhesion assays. In these assays equal numbers of knockdown cells were plated on type I collagen or fibronectin-coated wells. After allowing adhesion and spreading for 30 and

60 min, a profound decrease in the number of attached cells was observed for Tns3-depleted cells (Fig. 4C). This decrease was observed by all applied *Tns3* shRNAs and was evident on both substrates. A similar albeit less pronounced decrease of cell adhesion was also seen in HCT8 colon cancer cells upon stable Tns3-knockdown (Fig. S3). The MDA-MB-468-knockdown cells which remained attached lacked Tns3-positive cell–matrix adhesions and covered a smaller area on collagen than the control cells, suggestive of an impaired spreading behavior (Fig. 4D,E). The reduced cell size could be verified by transient knockdown using specific *Tns3* siRNAs (Fig. S4). In addition, we performed a transwell migration assay to examine the migratory capacity. Even without chemotactic stimulation, the undirected migration of Tns3-depleted cells was slightly but significantly decreased (Fig. 4F). By using EGF as a chemotactic stimulus, we further observed that the migratory activity of Tns3-knockdown cells was strongly decreased compared to control cells. Hence, knockdown of Tns3 impaired
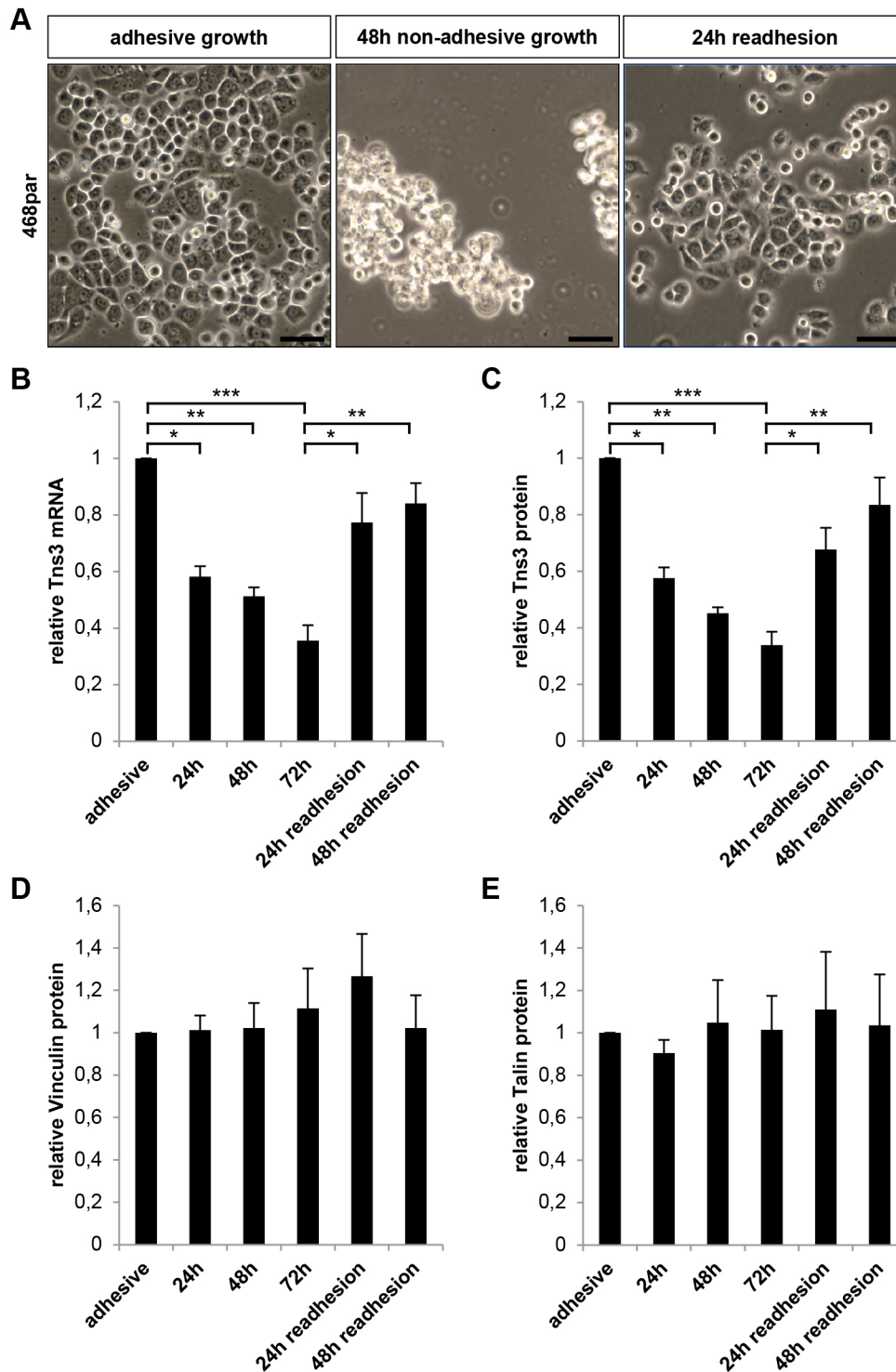
Fig. 3. Adhesion-dependent expression of Tns3 in MDA-MB-468 cells. (A) 468par cells were non-adhesively cultivated on polyHEMA-coated dishes for up to 72 h. Afterwards cells were allowed to re-adhere to normal culture dishes. Phase-contrast micrographs of cells at the times indicated. Scale bars: 50 µm. (B) *Tns3* mRNA transcript levels were determined by qRT-PCR, and normalized to ALAS1 and HPRT1 expression. (C) Quantification of Tns3 protein levels in total cell lysates under indicated conditions normalized to tubulin. (D) Quantification of vinculin protein levels in total cell lysates under indicated conditions normalized to tubulin. (E) Quantification of talin protein levels in total cell lysates under indicated cells normalized to tubulin. All error bars represent ±s.e.m., n=3. All P-values were calculated by Tukey's post-hoc test using one-way ANOVA (*P≤0.05, **P≤0.01, ***P≤0.001).

migration of MDA-MB-468 cells in both unstimulated and EGF-stimulated conditions.

To examine the underlying structural changes of cell–matrix contacts, we analyzed the immunofluorescence pattern of the focal adhesion proteins vinculin, talin and paxillin in cells that adhered despite Tns3-knockdown. For this purpose, Tns3-depleted and control cells were allowed to adhere and spread out for 15 min, 30 min and 60 min on collagen-(Fig. 5) or fibronectin-coated coverslips (data not shown). In cells transfected with a control shRNA, the proteins vinculin and paxillin were detected in the

typical dot-like focal adhesions at the tip of F-actin fibers (Fig. 5A). Methanol/acetone fixation also revealed a similar localization for talin (Fig. 5B). All three focal adhesion proteins were located at the moving front of the spreading control cells. In contrast, the Tns3-depleted cells displayed an altered localization and appearance of focal adhesion proteins, and diminished spreading. Vinculin, paxillin and also talin appeared to mainly accumulate at peripheral positions in thick focal adhesion plaques in Tns3-knockdown cells (Fig. 5, right panels). Colocalizing with the deformed adhesion sites, Tns3-depleted cells showed strong cortical
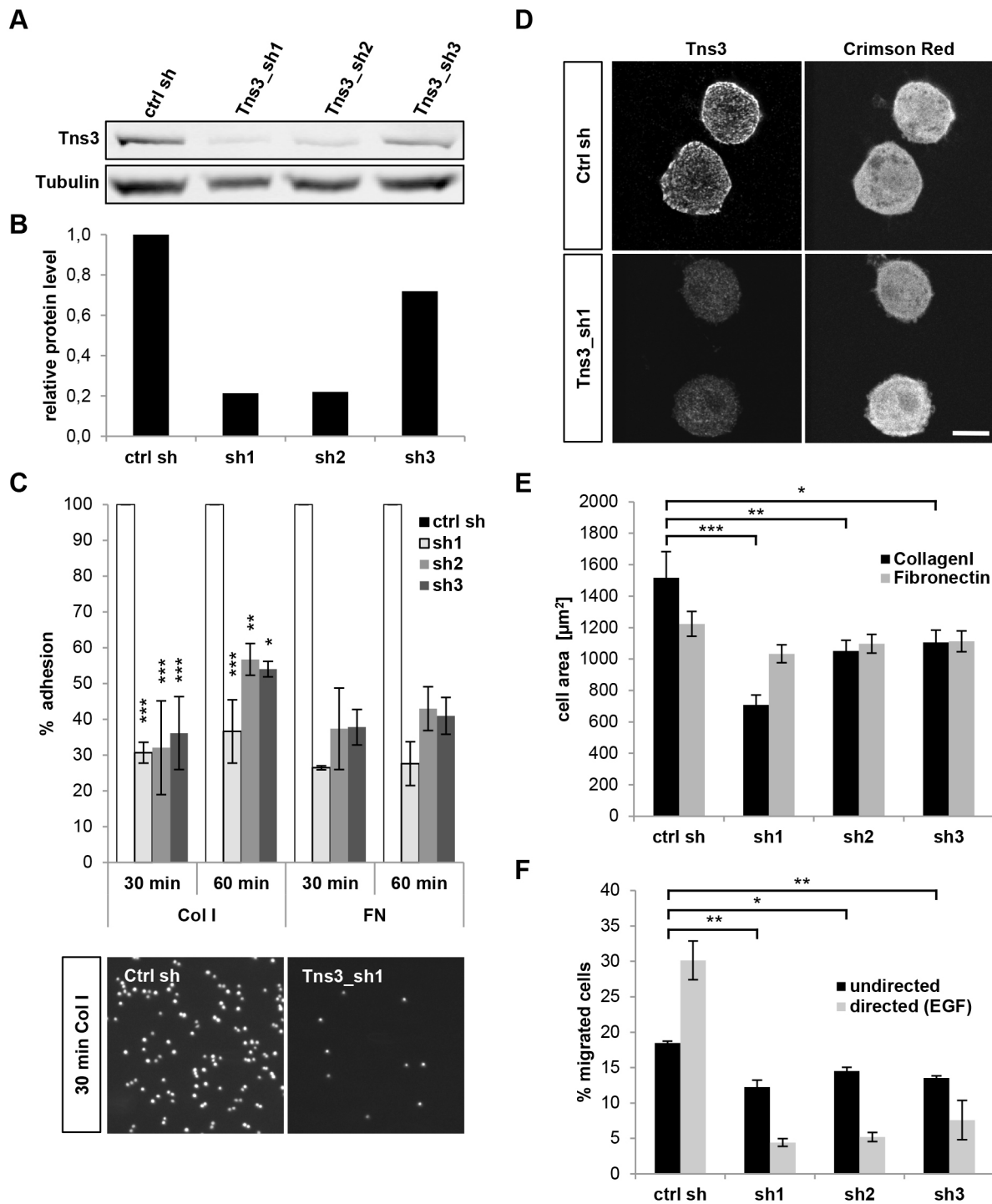
Fig. 4. Adhesion and migration of MDA-MB-468 cells upon stable Tns3-knockdown. Three different *Tns3*-targeting shRNA constructs (Tns3_sh1, Tns3_sh2, Tns3_sh3) were lentivirally transduced and resistant cells were selected with puromycin (2 µg/ml). As control, a non-targeting sequence (ctrl sh) was used. (A) Representative western blot showing levels of total Tns3 and tubulin in stable cell lines. (B) Quantification of Tns3 protein levels in total cell lysates from indicated cells normalized to tubulin. (C) Adhesion of stable cell lines to collagen (Col I)- or fibronectin (FN)-coated surfaces for the indicated times. Shown is the percentage of adhered cells normalized to the control (Col: n=3, FN: n=2). Representative images of DAPI-stained cells plated on type I collagen for 30 min before fixation are shown below. (D) Representative images of cells cultivated overnight on collagen, followed by immunostaining of Tns3. Stable transduction is indicated by Crimson Red expression. Scale bar: 10 µm. (E) Cell area determination by automated tracking of 50–100 cells per condition. Cells were seeded on coated 8-well chamber slides for 30 min before spreading of individual living cells was monitored over 15 h. (F) Transwell cell migration for 22 h with or without EGF as a chemoattractant, normalized to the seeding controls. The error bars represent ±s.e.m., n=3. All P-values were calculated by Tukey's post-hoc test using one-way ANOVA (*$P \leq 0.05$, **$P \leq 0.01$, ***$P \leq 0.001$).

F-actin staining around the cell periphery. In those Tns3-depleted cells that still adhered to the matrix, any further processing of the initial focal adhesions into more mature structures seems impaired.

Automated measurements of paxillin-positive structures showed a reduction of focal adhesions per cell to around 50% upon Tns3-knockdown (Fig. 5C). Whereas the mean area covered by individual
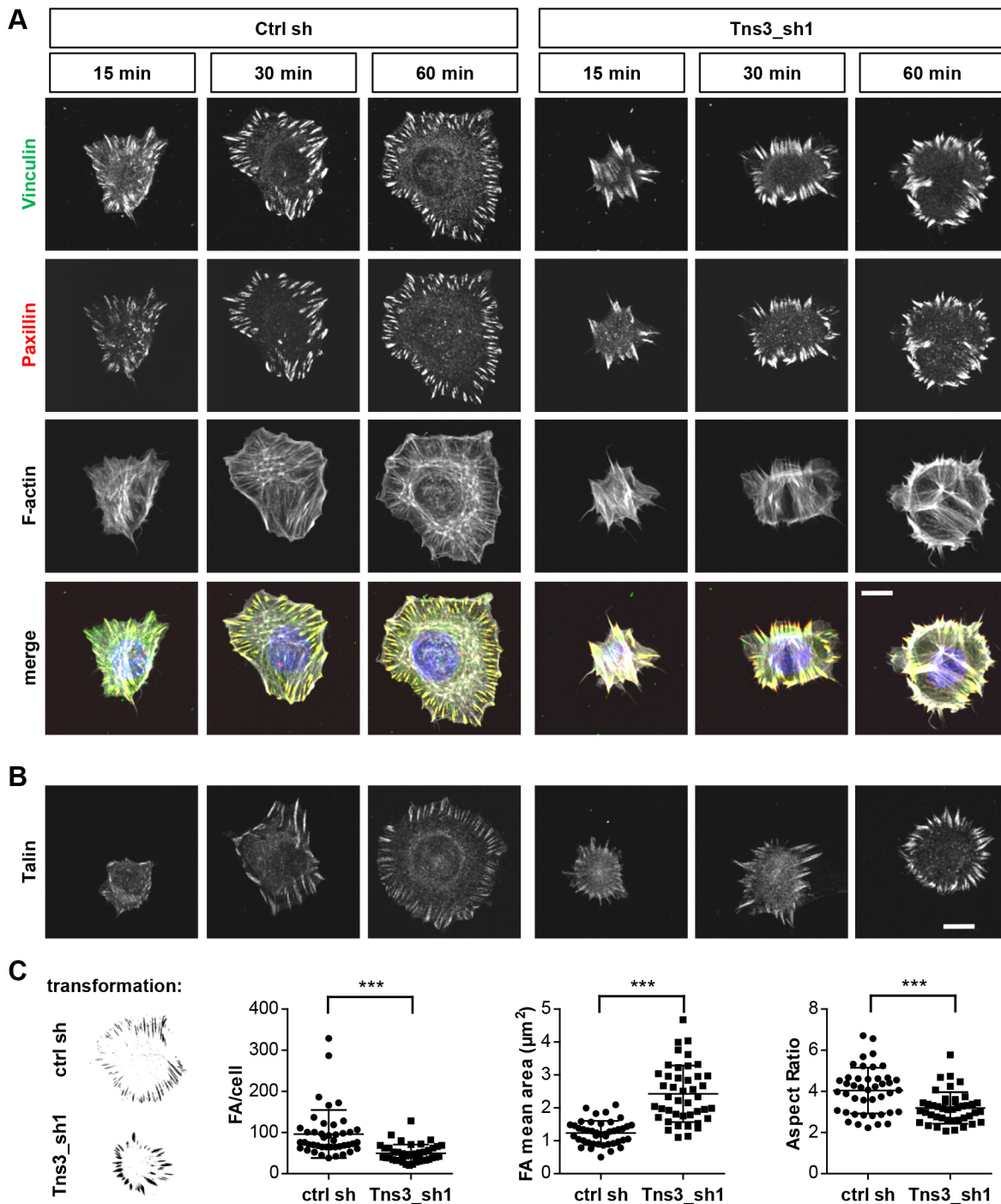
Fig. 5. Tns3-knockdown results in altered focal adhesion formation. Stable Tns3-knockdown cells (Tns3_sh1) and ctrl shRNA cells (Ctrl sh) were plated on collagen-coated glass slides, stained for the indicated proteins and analyzed by fluorescence confocal microscopy. Representative images are shown. Scale bars: 10 μm. (A) Co-immunostaining of vinculin (green), paxillin (red) and F-actin (SiR-Actin, depicted in white). Cells were fixed by formaldehyde 15, 30 and 60 min after seeding. Merged images show false color overlay (blue: DNA). (B) Talin immunostaining following MeOH/acetone fixation. (C) Number, size and aspect ratio of paxillin-positive focal adhesions from 43 Tns3-knockdown and control cells after 60 min of adhesion. Calculations were done after binarized image transformation (examples in left panels) and automated measurement. Scatter plots show FA number, mean area and mean aspect ratio per cell, with average ±s.d. indicated. Statistical significance according to unpaired two-sample Student's t-test (***$P \leq 0.001$).

focal adhesions significantly increased, the aspect ratio decreased – an indication of abnormal bundling or thickening of the adhesion sites (Fig. 5C). Together, these results suggest that reduction of Tns3 affects the dynamic of focal adhesion remodeling during spreading. This defect in focal adhesion maturation may be responsible for rounding and the reduced size of Tns3-deficient cells.

Tns3 rescues the restored adherent growth of 468^{susp} cells

We have shown that Tns3 is directly regulated by the status of adhesion and is lost in non-adherent 468^{susp} cells. Next, we asked whether exogenous expression of full-length Tns3 is able to restore adherent growth of the 468^{susp} cells. To address this question, suspension cells were transfected with plasmids containing either

GFP-tagged Tns3 or a GFP alone, followed by Geneticin (G418) selection. Immunoblot analysis revealed that selected cells showed an approximately three-fold overexpression of Tns3 compared to the parental cells (Fig. 6A). During the selection procedure both floating and adherent cells were cultivated. After 3 weeks of antibiotic selection, the number of adherently growing cells was determined. Importantly, we found ∼20-fold more adherently growing cells expressing GFP-Tns3 than those expressing GFP alone (Fig. 6B). Despite potential overexpression artefacts, this result suggested that re-expression of Tns3 in 468^{susp} is sufficient to revert to the non-adherent phenotype of these cells. Moreover, localization of Tns3-GFP into focal contacts was indistinguishable from the 468^{par} cells as shown by confocal microscopy (Fig. 6D). Furthermore, 468^{susp} cells stably overexpressing Tns3-GFP displayed an F-actin cytoskeleton architecture that is similar to 468^{par} cells. Moreover, they were able to restore the formation of F-actin fibers as well as the localization of vinculin to focal-adhesion-like structures (Fig. 6D). In contrast, 468^{susp} cells completely failed to attach and, hence, did not show any focal contacts (data not shown).

Cell−matrix adhesion is an important feature of cell migration and motility. Therefore, we next analyzed whether the Tns3-GFP-mediated re-adhesion alters the migratory activity of 468^{susp} cells in a transwell migration assay. The cell migration of 468^{susp} cells that stably express Tns3-GFP was significantly increased compared to 468^{susp} control cells (Fig. 6C). Compared to 468^{par} cells, however, cell migration was only partially restored by Tns3-GFP, possibly because either overexpression of Tns3-GFP or additional alterations in the selected suspension cells. Nevertheless, our results show that Tns3-GFP expression restores cell adhesion of 468^{susp} cells and enhances their migratory activity.

DISCUSSION
Generation of MDA-MB-468^{susp} cells
In this study, we report on the regulation and role of the cell−matrix contact protein Tns3 in breast cancer cells during adhesion plasticity. We show that Tns3 expression is directly correlated with the status of cell adhesion and is lost following loss of cell−matrix adhesion in MDA-MB-468^{susp} cells, an enriched and stable subpopulation of MDA-MB-468 breast cancer cells growing in suspension.
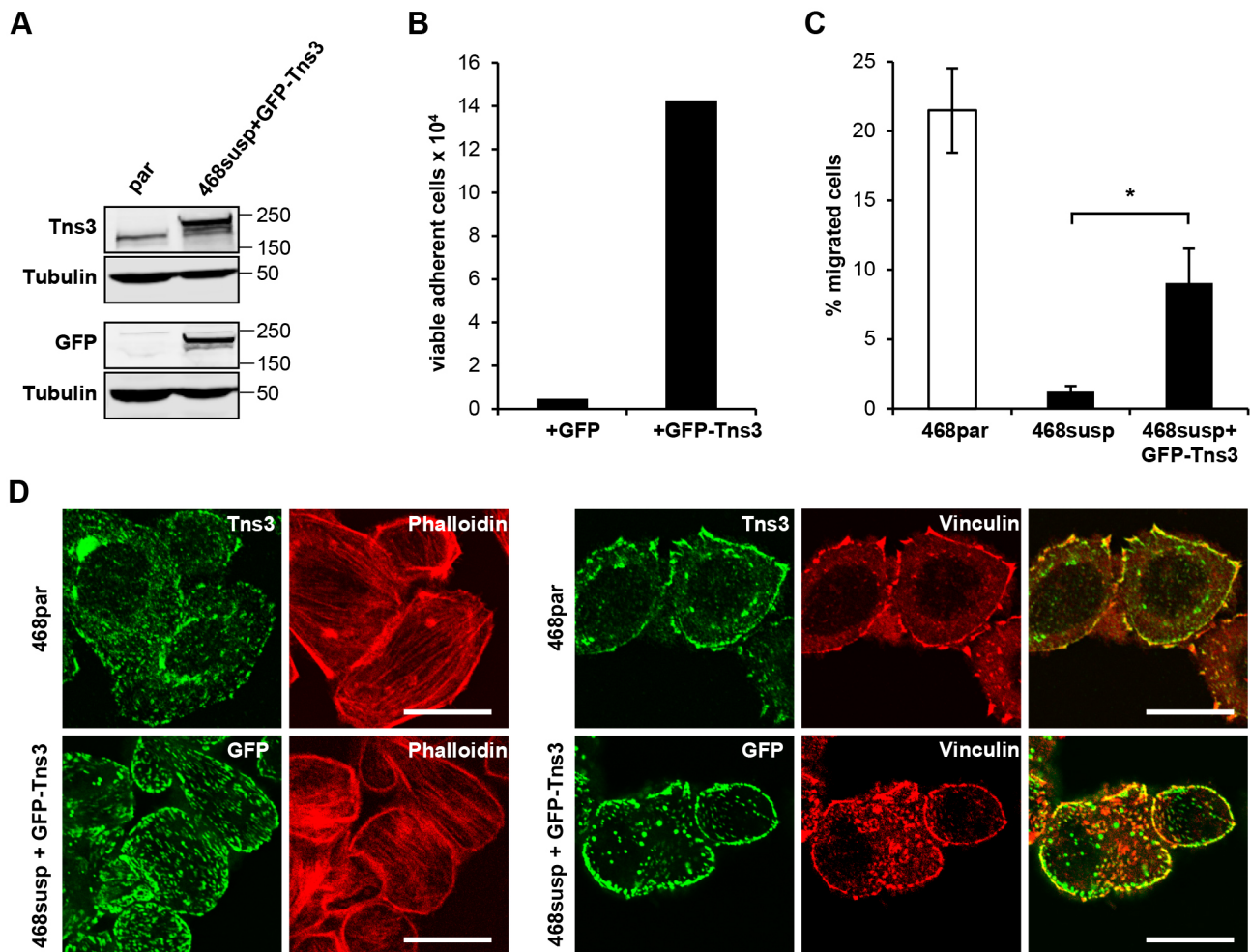

Fig. 6. Tns3 overexpression restored adherent growth of 468^{susp} cells. MDA-MB-468^{susp} cells were stably transfected with GFP-tagged Tns3 or with the pEGFPc1 vector as a control. During the selection procedure both non-adherent and adherent cells were cultivated. (A) Representative immunoblots of total cell lysates using Tns3- and GFP-specific antibodies. Tubulin was used as a loading control. (B) Number of adherently growing cells after 3 weeks of selection. (C) Transwell migration of 468^{par}, 468^{susp} and 468^{susp} cells expressing GFP-Tns3, measured after 22 h with EGF as a chemoattractant and normalized to the seeding controls. All error bars represent ±s.e.m., n=4. *P≤0.05 according to unpaired two-sample Student's t-test. (D) 468^{par} and 468^{susp} cells expressing GFP-Tns3 were stained for Tns3 (green) together with F-actin (phalloidin, red) or vinculin (red, right panels). Merged images show endogenous Tns3 or GFP-Tns3 (green) and vinculin (red). Scale bars: 10 μm.

Culturing cells in or on non-adhesive substrates can induce adhesion-independent growth of cells that typically grow as an adherent culture, such as epithelial cells. In doing so cells are forced to grow without substrate attachment and cell−matrix contacts, which results in a constrained suspension phenotype. However, in our study we aimed to establish a method that considers the inherent status of cell−matrix adhesion but still reflects adhesion plasticity, i.e. shows adherent and non-adherent growth. To this end, we have successfully generated non-adherently growing suspension sub-lines of MDA-MB-468 breast cancer cells which do not display obvious signs of genetic drift, as confirmed by identical STR analysis (data not shown). These suspension subcultures were acquired by enriching non-adherent single cells that spontaneously dissociated from MDA-MB-468 monolayer cultures. In a similar, approach Tang et al. generated an *in vitro* metastasis model consisting of metastasis-like dissociated round cells (R-cells) and adherent epithelial cells (E-cells) from HCT8 colon adenocarcinoma cells (Tang et al., 2010, 2014). In HCT8 colon cancer, R-cells occurred at very low frequency but the R-cell:E-cell ratio could be increased by appropriate physical properties of the culture substrate. In our study we were able to achieve stable suspension MDA-MB-468 subcultures after repeatedly separating and enriching non-adherent cells. It is remarkable that this non-adherent cell population is neglected in most studies that use MDA-MB-468, since non-adherent cells normally are discarded by medium aspiration. Presumably, also other cancer cell lines contain non-adherent subpopulations that are not taken into account by many experimental approaches. In contrast, we place the suspension phenotype of MDA-MB-468 cells into the spotlight and utilize it to investigate adhesion plasticity in human breast cancer cells.

After losing cell−matrix adhesion or sensing inappropriate cell−matrix contacts, epithelial cells normally undergo apoptotic cell death − a process known as anoikis (Frisch and Francis, 1994; Frisch and Screaton, 2001; Gilmore, 2005). In tissue homeostasis, anoikis can be seen as a self-defense strategy that prevents cells losing ECM contact from dysplasia formation and metastatic dissemination (Guadamillas et al., 2011). However, many cancerous cells are able to avoid anoikis and have developed anoikis-resistance (Frisch and Screaton, 2001; Simpson et al., 2008; Taddei et al., 2012; Paoli et al., 2013; Buchheit et al., 2015). In this regard, the generation of non-adherent 468^susp was achievable because MDA-MB-468 cells are cancer cells whose loss of SMAD4 and subsequent caspase signaling was proposed to render them anoikis-resistant (Ramachandra et al., 2002). Furthermore, we observed, in both 468^susp and polyHEMA-induced suspension of 468^par, that cells form prominent cell-cell contacts and grow in grape-like structures. Tight cell-cell contact formation is a typical phenomenon of epithelial cells in suspension and has been discussed as compensatory mechanisms to prevent apoptosis after loss of cell-ECM adhesion (Kantak and Kramer, 1998; Zhan et al., 2004; Hofmann et al., 2007). Notably, although the protein levels of the cell-cell contact protein E-cadherin are fairly similar, E-cadherin localizes more prominently to cell-cell contacts in 468^susp than in 468^par cells (Fig. S5C,D). Moreover, an adaptation or compensation of 468^susp towards a more robust anoikis-resistance is indicated also by the increased expression of the cell-cell contact protein CEACAM6 (Fig. S5A,B), which has been shown to increase anoikis-resistance in carcinoma cells (Ordonez et al., 2000; Duxbury et al., 2004).

Tns3 is lost in MDA-MB-468^susp cells and directly regulated by cell−matrix adhesion

To examine the impact of adhesion plasticity on gene regulation in breast cancer cells we tested the differential gene expression between 468^par and 468^susp cells by using microarrays. We found that, in suspension cells, the cytoskeletal adapter protein Tns3 is strongly reduced on both mRNA and protein levels. Loss of Tns3 mRNA and protein is directly caused by loss of cell−matrix adhesion but restored by gain of cell−matrix adhesion, as corroborated by short-term cultures of 468^par on non-adhesive polyHEMA substrate. Furthermore, the adhesion-mediated regulation of Tns3 is not restricted to MDA-MB-468 cells since other breast cancer cells, such as MCF7, as well lose Tns3 expression after loss of cell−matrix adhesion (Fig. S3). Although it seems reasonable that non-adherent cells downregulate focal adhesion proteins, our data clearly show that other main cell−matrix adapter proteins, such as vinculin and talin, are not affected by loss of cell−matrix adhesion. This result might be explained by the proposed role of Tns3 in late cell−matrix contacts, whereas vinculin and talin are important in early and intermediate focal adhesions (Zamir et al., 1999, 2000; Katz et al., 2000; Zaidel-Bar et al., 2003, 2004). In this regard, it is conceivable that cells retain the expression of early adhesion proteins, while they shut down expression of late adhesion proteins that miss the right chemical or physical signal from early adhesion. However, our results show less-dramatic effects for Tns2 and Tns1. Hence, the adhesion-mediated regulation of Tns3 might be an isoform-specific effect.

We have demonstrated that cell−matrix adhesion regulates Tns3 expression. However, we also show that Tns3 itself influences the adhesion properties of MDA-MB-468 cells. In Tns3-knockdown experiments, we show that matrix adhesion including cell spreading dynamics and focal adhesion composition, are impaired in 468^par cells after stable shRNA-mediated Tns3-knockdown. In Tns3-deficient cells that still adhere, the correct adhesion maturation from early into late adhesions seems impeded. This finding is in accordance with work from Pankov et al. which shows that−when the Tns function in human fibroblasts is interrupted − late fibrillar adhesions disappeared but early focal adhesions stayed intact, thereby indicating that Tns is necessary for adhesion maturation (Pankov et al., 2000). Furthermore, we found that knockdown of Tns3 decreases the migratory activity in MDA-MB-468 cells, a finding that could be related to the impeded adhesion maturation. This result coincides with two other studies that reported reduced cell migration in four carcinoma cell lines, including MDA-MB-231 and MDA-MB-468 cells, after Tns3-knockdown (Qian et al., 2009; Shinchi et al., 2015). In contrast, Katz et al. and Cao et al. showed that Tns3-knockdown in non-tumorigenic mammary MCF 10A cells results in increased migration behavior (Katz et al., 2007; Cao et al., 2012). In these studies, EGF treatment was proven to strongly increase the migration of MCF 10A cells (Katz et al., 2007; Cao et al., 2012). Similarly, EGF induced cell migration of MDA-MB-468 cells in our experiments. However, it was unexpected that EGF intensified the Tns3-knockdown-mediated decrease in cell migration of MDA-MB-468 cells. In this context, it is important to note that EGF itself has been shown to decrease Tns3 but to increase levels of Tns4 (Cten) in MCF 10A cells and, therefore, causes a Tns3-to-Tns4 switch in these non-tumorigenic cells (Katz et al., 2007). Remarkably, we also found a Tns3-to-Tns4 switch in MDA-MB-468 cells. However, the Tns3-to-Tns4 switch in MDA-MB-468 cells occurred independently of EGF treatment but as a function of cell−matrix adhesion. Although loss of cell−matrix adhesion decreased Tns3 levels in 468^susp it significantly increased Tns4 mRNA and protein levels. Interestingly, a 7-fold increase oTns4 induced by loss of cell−matrix adhesion has also been shown in the HCT8 colon cancer R-cell−E-cell (R-E) model by Tang et al. (2014). We observed that Tns3-knockdown reduced matrix

adhesion of HCT8 cells (Fig. S3), but it is unclear whether Tns3 is altered in the R-E model. Whether the adhesion-mediated and the EGF-mediated Tns3-to-Tns4 switches share the same molecular downstream mechanisms needs to be addressed in further studies.

Tns3 is a target and regulator of cell–matrix adhesion

Tns3 directly links β-subunit integrins with the F-actin cytoskeleton (Lo, 2004) and has obviously been named by its key function: maintaining cellular tension. In our study, we show that not just Tns3 is responsible for maintaining correct cell–matrix adhesion (and, therefore, tension) but that, vice versa, cell–matrix tension is crucial for *Tns3* expression. Hence, we propose a *Tns3* feedback loop in which correct cell–matrix adhesion and *Tns3* expression are tightly intertwined in breast cancer cells (see Fig. 7). Loss of cell–matrix adhesion results in the disappearance of Tns3. In turn, loss of Tns3 impairs cell–matrix adhesion as shown by our Tns3-knockdown experiments and, together with other changes, maintains loss of cell–matrix adhesion. Once cells have left the Tns3 feedback loop and lost cell–matrix adhesion Tns4 becomes upregulated. Although Tns4 is able to bind to the β-subunit of integrins, it lacks the actin-binding domain of the larger Tns isoforms (Lo and Lo, 2002; Lo, 2004) and, therefore, is unable to mediate cell–matrix adhesion. Hence, it is conceivable that the upregulated Tns4 contributes to suppression of *Tns3* expression and keeps suspension cells outside the Tns3-feedback loop. In addition, we have shown that cell–matrix adhesion can be partially restored in non-adherent 468[susp] cells when GFP-Tns3 is overexpressed. This finding corroborates our conclusion that Tns3 and cell–matrix adhesion are mutually dependent in MDA-MB-468 breast cancer cells. It remains to be investigated whether such mutual regulation plays a role during cycles of metastatic dissemination through the bloodstream and colonization at distal sites, when cancer cells, respectively, diminish and regain adhesive properties. Moreover, tensins have originally been identified as a protein family with structural functions and Tns3 is also an important docking platform for signaling molecules. In this regard, Tns3 was shown to bind several pro-oncogenic tyrosine phosphorylated proteins, including p130Cas, Sam68, Src and FAK (Cui et al., 2004; Defilippi et al., 2006; Mitra and Schlaepfer, 2006; Qian et al., 2009). Additionally, Tns3 can bind deleted in liver cancer 1 (DLC1) and dedicator of cytokinesis protein 5 (DOCK5), both of which are components of the Rho GTPase pathway (Cao et al., 2012; Touaitahuata et al., 2016; Blangy, 2017). Therefore, the adhesion-mediated Tns3 regulation is likely to entail strong consequences on downstream signaling involved in the fate of cancer cells.

MATERIALS AND METHODS
Plasmids and reagents
Human full-length *Tns3* was cloned into pEGFPc1 (Clontech, Mountain View, CA) for mammalian expression. shRNA construct (Tns3_sh1: 5′-G-CATCACCCTGACAGACAATCTTCAAGAGAGATTGTCTGTCAGG-GTGATGCTTTTTTACGCGT-3′, Tns3_sh2: 5′-GGACGCATAGGAG-TGGTCATATCATTTCAAGAGAATGATATGACCACTCCTATGCGT-CCTTTTTTACGCGT-3′, Tns3_sh3: 5′-GAAAGCTGGAGATTTGGC-CAATGAATTCAAGAGATTCATTGGCCAAATCTCCAGCTTTCTTTT-TTACGCGT-3′, ctrl_sh 5′-TTGTACTACACAAAAGTACTGTTCAAGA-GACAGTACTTTTGTGTAGTACAATTTTTTACGCGT-3′) were cloned in pLVX-shRNA2 Crimson kindly provided by Stefan Hüttelmaier. This vector is based on pLVX-shRNA2 (Clontech Laboratories, Mountain View,
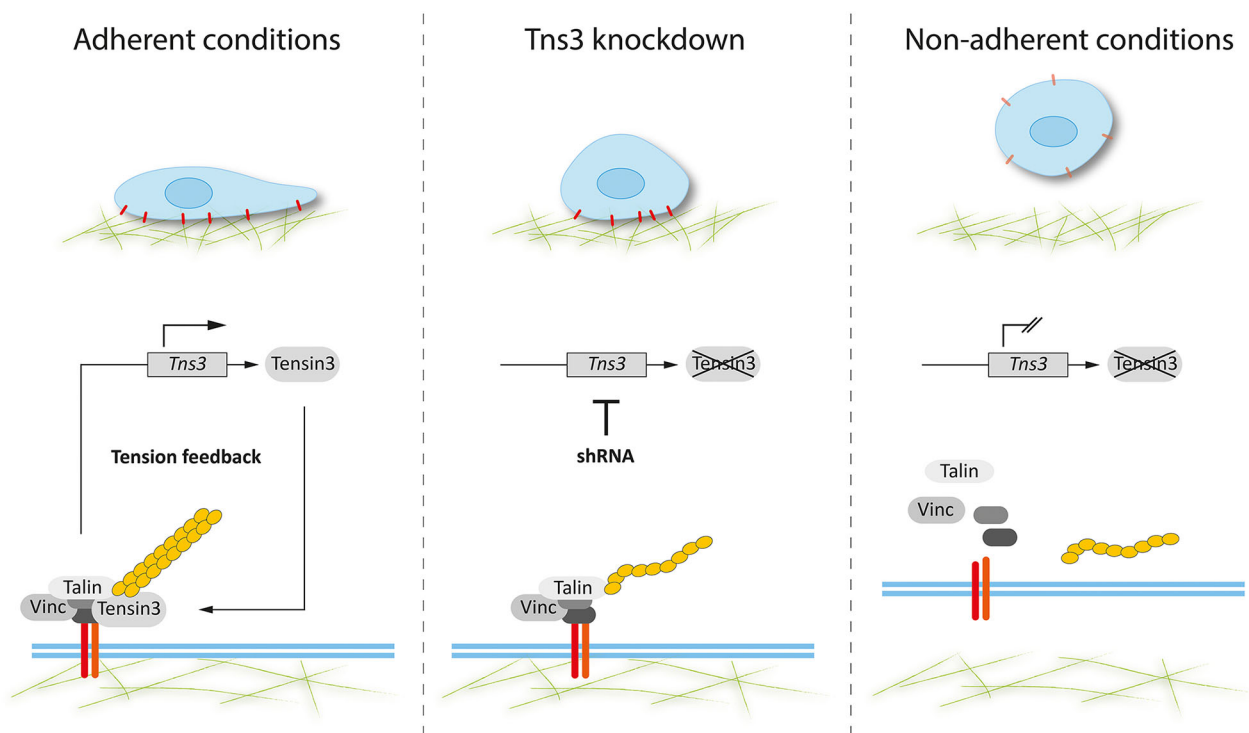

Fig. 7. Model of the interplay between Tns3 expression and cell–matrix adhesion. During adherent conditions cells attach via integrin-containing cell–matrix contacts (red) to the substrate (green fibers). This results in a positive feedback signal necessary for *Tns3* gene expression. In turn, Tns3 protein is expressed and contributes to correct cell–matrix contacts by connecting integrins (orange, red) to the actin cytoskeleton (yellow). This feedback loop can be disturbed by either loss of *Tns3* gene expression or loss of cell–matrix adhesion. Loss of *Tns3* expression by i.e. RNAi leads to the disappearance of the Tns3 protein. Consequently, cell adhesion, migration and focal adhesion formation are impaired. On the other side, loss of cell–matrix adhesion prevents the required positive feedback from adhesion and results into a shutdown of the *Tns3* expression and Tns3 protein production.

CA). The ZS Green was replaced by E2-Crimson, a far-red fluorescent protein. The siRNAs were purchased as siRNA duplexes from Sigma-Aldrich (Steinheim, Germany). The sequences were: siTns3-1 5′-CCAGG-CCCUUGACAGGUUU-3′, siTns3-3 5′-GGACAAUGCCAGCAAAGAU-3′, siTns3-5 5′-GGUUGUAGCUCACCAGUAU-3′ and siTns3-9 5′-GCU-CGAAUGAACCAUAUUU-3′. As control, *Silencer* Negative Control #1 siRNA (Thermo Fisher Scientific, cat. no. AM4636) was used. For microarray analysis the Human Gene ST 1.0 array, comprising 28.869 probe sets covering the entire transcriptome was used. The labeling, hybridization and quality control was carried out as described (Descot et al., 2009). The data were analyzed in collaboration with Reinhard Hoffmann (Institute of Laboratory Medicine, Augsburg Hospital, Germany), by using RMA normalization and the permutation-based SAM algorithm. The q-value is the lowest false discovery rate at which the gene is called significant, applying a threshold of 4.62%. Microarray datasets have been deposited at the Gene Expression Omnibus database (accession number GSE98062).

Primary antibodies used were anti-GFP (1:1000; Sigma, catalog no. G1544), anti-GST (1:3000; Sigma, catalog no. G7781), anti-vinculin (1:5000; Sigma, catalog no.V9131), anti-talin (1:4000; Sigma, catalog no. T3287), anti-tubulin (1:2000; Sigma, catalog no. T9026), anti-Tns3 (1:1000; Millipore, catalog no. ABT29), anti-FAK (1:1000; Millipore, catalog no. 06-543), anti-Tns1 (1:500; abcam, catalog no. ab135882), anti-paxillin (1:1000; abcam, catalog no. ab32084), anti-Tns2 (1:500; Cell Signaling, catalog no. 11990), anti-Tns4 (1:1000; Abnova, catalog no. H00084951-MO), anti-Rac1 (1:1000; BD bioscience, catalog no. 610650), anti-E-cadherin (1:1000; BD Bioscience, catalog no. 610181), anti-integrinβ1, β3, β4 and α2, α5, α6, αV (1:20 for flow cytometry all from Miltenyi Biotec, Bergisch Gladbach, Germany). F-actin was visualized with Atto 546 Phalloidin (Sigma-Aldrich) or SiR-Actin (Cytoskeleton, Denver, CO). Alexa-Fluor-conjugated (Alexa488, 546, 568; 1:200) and IRDye® (800CW, 680RD) secondary antibodies were from Thermo Fisher Scientific or Li-Cor (Bad Homburg, Germany), respectively. DNA was stained with DAPI (Sigma-Aldrich).

Cell culture and transfection
The breast cancer cell line MDA-MB-468 was cultured at 37°C under 5% CO$_2$ in RPMI medium supplemented with 10% (v/v) fetal calf serum (FCS) and Gibco© Antibiotic-Antimycotic (1%, Thermo Fisher Scientific, Schwerte, Germany). For non-adhesive growth, cell culture dishes were coated with 1.2% (w/v) poly(2-hydroxyethyl methacrylate) (pHEMA, Sigma-Aldrich) dissolved in ethanol. Dishes were air-dried for 12 h in a laminar flow hood under sterile conditions. MCF7 cells were grown in Dulbecco's modified Eagle's medium (DMEM) supplemented with high glucose (10% v/v) FCS, 1% sodium pyruvate (v/v) and Antibiotic-Antimycotic.

Transfections were carried out using Lipofectamine LTX (Thermo Fisher Scientific). 1 µg plasmid DNA was added to 5×10^5 468^{susp} cells (12-well plates) according to the manufacturer's instructions. Cells were selected by using 1 mg/ml Geneticin (G418, Thermo Fisher Scientific). Lentiviral transductions were done by adding concentrated virus titer and 10 µg/ml polybrene to 3×10^5 cells (12-well plates) for 24 h. Resistant cells were selected by using 2 µg/ml puromycin (Thermo Fisher Scientific). For virus production, HEK293T cells were co-transfected by CaPO$_4$ precipitation with pMD2.G (Addgene, no. 12259), psPAX2 (Addgene, no. 12260) both kindly provided by Stefan Hüttelmaier and pLVX-shRNA2 crimson containing either ctrl shRNA or Tns3-targeting sequence. Lentiviruses were purified 48 h post transfection by PEG6000 precipitation.

Quantitative RT-PCR
Endogenous target gene expression was analyzed following isolation of total RNA by using the RNeasy Mini Kit (Qiagen, Hilden, Germany). First-strand cDNA was synthesized from 500 ng RNA by using random hexamers and Verso cDNA Synthesis Kit (Thermo Fisher Scientific) according to the manufacturer's instructions. qRT-PCR was performed using 1.5 µl of 1:5 diluted cDNA, 0.5 mM primers and DyNAmo ColorFlash SYBR Green qPCR Kit (Thermo Fisher Scientific) in 10 µl reaction volume using LightCycler 480 II instrument (Roche, Basel, Schweiz). Primer sequences used were as follows: *HPRT1*, forward: 5′-CCTGGCGTCATTAGTGAT-

3′, reverse: 5′-AGACGTTCAGTCCTGTCCAATAA-3′, *ALAS1*, forward: 5′-CTGCAAAGATCTGACCCCTC-3′, reverse: 5′-CCTCATCCACGAA-GGTGATT-3′, *CEACAM6*, forward: 5′-CTCTACAAAGAGGTGGACAG-3′, *CEACAM6*, reverse: 5′-GTTAGAAGTGAGGCTGTGAG-3′, *Tns1*, forward: 5′-ACTACCTGCTGTTCAACCTC-3′, reverse: 5′-ATGACAAC-TCCTATCCTGCC-3′, *Tns2*, forward: 5′-TATACTGCAAGGGAAACA-AGG-3′, reverse: 5′-CTGCTGTTCATTCTGATGGAG-3′, *Tns3*, forward: 5′-CATTCATTGTTCGAGACAGCCA-3′, reverse: 5′-CAAATCTCCAG-CTTTCTTGTTCAG-3′, *Tns4*, forward: 5′-GAGAGCAAGCAATCGAG-CTG-3′, reverse: 5′-CAAAGTAGGGCTCCTCATCTG-3′, *Talin1*, forward: 5′-GAGTCAGTGTGCCAAGAACC-3′, reverse: 5′-GTACACTTCTCCAT-TGTCTCCC-3′, *Vinculin*, forward: 5′-GATGAGGCTGAGGTCCGTAA-3′, reverse: 5′-AGCTCCTGCTGTCTCTCGTC-3′. Relative gene expression levels were calculated according to the $2^{-\Delta\Delta CT}$ method. Results shown are averaged from at least three independent biological replicates.

Immunofluorescence and microscopy
For immunofluorescence analysis, 8×10^4 cells (12-well plates) were grown on glass coverslips coated with type I collagen (0.5 mg/ml) or fibronectin (0.1 mg/ml), fixed with 3.7% formaldehyde in PBS for 15 min, and permeabilized with 0.2% (v/v) Triton X-100 in PBS for 10 min. For talin immunostaining, cells were fixed and permeabilized for 10 min in ice-cold (−20°C) methanol/aceton (1:1). After blocking in PBS, 10% FCS, 1% BSA, 0.05% Triton X-100 for 30 min, primary antibodies were diluted 1:100 to 1:400 and applied for 1 h at room temperature. Alexa-Fluor 488- and -546-conjugated secondary antibodies were diluted 1:200 and applied for 1 h at room temperature. Samples were covered with ProLong Gold antifade reagent (Life Technologies) and imaged using a confocal microscope (TCS SP2 AOBS or SP5; Leica, Wetzlar, Germany) or an Apotome-containing Axio Observer.Z1 (Zeiss, Jena, Germany) equipped with 63× and 100× oil objectives and a monochrome Axiocam MRm camera. Representative images are shown.

For quantitative focal adhesion analysis, cells were allowed to adhere to collagen-coated glass slides for 60 min and followed by immunostaining for paxillin. 43 single cells from *n*=4 experiments were recorded by using a confocal microscope (SP5, Leica) with 100× oil objective. Paxillin fluorescent images were automatically batch processed and analyzed by using the open source software ImageJ (version 1.48u). First, background fluorescence was removed by substrate background with a 100-pixel rolling ball radius. Next, images were thresholded and binarized by the Otsu-Method. Finally, focal adhesion number and size area were analyzed above a lower threshold of 0.1 µm^2. The aspect ratio was calculated as major-axis/minor-axis of focal adhesions fitted ellipses.

For 2D single-cell area analysis, cells were seeded on collagen I or fibronectin-coated 8-well chamber slides (IBIDI). Cell attachment was allowed for 30 min before spreading was monitored over 15 h by time-lapse analyses (10 min/frame) based on E2-Crimson Red-fluorescence using a Leica SP5X inverse confocal microscope equipped with a Ludin cube life chamber, 40× oil objective and multi-positioning. Automated cell tracking was performed using the 'CellMigrationAnalyzer' tool of the MiToBo (http://www2.informatik.uni-halle.de/agprbio/mitobo/) package for ImageJ (http://imagej.nih.gov/ij/) to determine the mean area [µm^2] of those single cells observed over a time period of at least 6 h. A total of 50–100 cells per condition were analyzed.

Western blotting
Cells were washed twice with ice-cold phosphate-buffered saline and lysed in RIPA buffer [50 mM Tris-HCl, pH 7.4, 150 mM NaCl, 2 mM EDTA, 1% (v/v) Triton X-100, 0.1% SDS, Complete EDTA-free protease inhibitor cocktail] for 30 min on ice. The proteins were separated on SDS-PAGE, transferred to polyvinylidene fluoride (PVDF) membranes (Merck Millipore), incubated with indicated primary antibodies used at 1:200–1:5000 dilutions and incubated overnight at 4°C. Fluorophore-labeled secondary antibodies used at 1:15,000 dilution (LI-COR, Bad Homburg, Germany) were incubated for 1 h at room temperature. The fluorescence signals were detected with ODYSSEY CLx (LI-COR) and quantified by the associated software. Quantitative results were calculated from at least three independent biological experiments.

Quantification of active Rac1

Preparation of the GST−PAK−CRIB fusion protein was carried out as described by Busche et al. (2008). 4×10^6 MDA-MB-468[par] or -468[susp] cells were seeded in 15 cm dishes and cultured for 24 h. Afterwards, cells were lysed in 1 ml Rac lysis buffer (50 mM Tris pH 7.5, 1% Triton X-100, 150 mM NaCl, 10 mM $MgCl_2$, 0.5% sodium desoxycholate, 0.1% SDS, protease inhibitors). Equal amounts of protein lysates (1 mg) were incubated with immobilized GST−PAK−CRIB, rotated at 4°C for 60 min, followed by washing in Rac wash buffer (3×)(50 mM Tris pH 7.5, 1% Triton X-100, 150 mM NaCl, 10 mM $MgCl_2$, protease inhibitors). Bound proteins were detected by western blotting using Rac1, GST and tubulin antibodies. Quantitative results of active pulled-down Rac1 levels were calculated and normalized to Rac1 in total lysates (normalized on tubulin).

Cell motility assay

Migration assays were performed in transwell diffusion chambers (Corning Costar, Corning, NY) with a pore size of 8 µm as described previously (Wulfaenger et al., 2008). 600 µl RPMI1640 medium containing 10% FCS (optionally containing 50 ng/ml EGF) were added to the bottom of the 24-well plate. 4.5×10^4 cells were inserted into the top chamber. After 22 h at 37°C, the upper side of the membrane was wiped to remove all remaining cells. The number of migrated cells was determined in a CellTiter-Glo Luminescent Cell Viability Assay (Promega, Madison, WI) according to the manufacturer's protocol. Luminescence was measured by using a GloMax 96 Microplate Luminometer (Promega). Results are expressed as the percentage of migrated cells compared to the total number of cells.

Cell viability assay

2×10^4 cells were seeded in a 96-well microplate for indicated time periods. Proliferation was determined with Colorimetric Cell Viability Kit I (PromoKine, Heidelberg, Germany) according to the manufacturer's protocol. Absorbance at 450 nm was measured after 1.5 h of incubation at 37°C using a microplate reader.

Apoptosis assay

1×10^6 cells were subjected to the EnzChek Caspase-3 Assay Kit #2 (Thermo Fisher Scientific) according to the manufacturer's protocol. Absorbance at 520 nm was measured after 30 min of incubation at room temperature by using a microplate reader.

Adhesion assay

For cell-substratum adhesion assays, 96-well tissue culture plates were coated with type I collagen (0.5 mg/ml) or fibronectin (0.1 mg/ml) in PBS at RT overnight, rinsed twice with PBS, and cells were then allowed to adhere to the coated surface for 30 min or 60 min, respectively. To remove non-adherent cells, wells were washed twice with PBS. DNA was stained with DAPI. Fluorescence was measured using a ClarioStar High Performance Monochromator Multimode Microplate Reader (BMG LABTECH, Ortenberg, Germany).

Collagen contraction assay

Increasing cell numbers (1×10^4, 3×10^4, 5×10^4 and 10×10^4) of MDA-MB-468[par] or -468[susp] cells were mixed with type I collagen (final concentration 1.5 mg/ml) in RPMI1640 medium containing 10% FCS and 10 ng/ml EGF and allowed to solidify in 96-well plates. For the negative control collagen I was mixed only with the according medium. After 1 h incubation at 37°C 200 µl RPMI1640 medium containing 10% FCS and 10 ng/ml EGF were added to each well. The collagen lattices were detached from the surface of the well and after 4 days incubation at 37°C the total area covered by the collagen lattices was measured and compared to that of the negative control. Results show the shrinkage of the collagen gel in %.

Flow cytometry

5×10^5 cells were centrifuged at 300 g for 10 min. Cells were resuspended in 100 µl PBS (pH 7.2) containing 0.5% BSA and 2 mM EDTA, and incubated for 10 min at 4°C with 5 µl anti-integrin β1, β3, β4 and α2, α5, α6, αV antibodies conjugated to FITC or PE (1:20; Miltenyi Biotech, cat. nos:

130-101-256, 130-100-160, 130-101-436, 130-100-337, 130-097-225, 130-097-246, 130-100-704). Cells were washed by adding 1 ml of PBS and resuspended in 100 µl PBS. Fluorescence was measured using a BD Acccuri Flow Cytometer. Integrin surface levels in 468[susp] cells were compared to those in MDA-MB-468[par] cells.

Data availability

Microarray datasets have been deposited at the Gene Expression Omnibus database under accession number GSE98062 (https://www.ncbi.nlm.nih.gov/geo/query/acc.cgi?acc=GSE98062).

Supplementary information

Supplementary information available online at http://jcs.biologists.org/lookup/doi/10.1242/jcs.200899.supplemental

References

Blangy, A. (2017). Tensins are versatile regulators of Rho GTPase signalling and cell adhesion. *Biol. Cell* **109**, 115-126.

Buchheit, C. L., Angarola, B. L., Steiner, A., Weigel, K. J. and Schafer, Z. T. (2015). Anoikis evasion in inflammatory breast cancer cells is mediated by Bim-EL sequestration. *Cell Death Differ.* **22**, 1275-1286.

Busche, S., Descot, A., Julien, S., Genth, H. and Posern, G. (2008). Epithelial cell-cell contacts regulate SRF-mediated transcription via Rac-actin-MAL signalling. *J. Cell Sci.* **121**, 1025-1035.

Calderwood, D. A., Fujioka, Y., de Pereda, J. M., Garcia-Alvarez, B., Nakamoto, T., Margolis, B., McGlade, C. J., Liddington, R. C. and Ginsberg, M. H. (2003). Integrin beta cytoplasmic domain interactions with phosphotyrosine-binding domains: a structural prototype for diversity in integrin signaling. *Proc. Natl. Acad. Sci. USA* **100**, 2272-2277.

Cao, X., Voss, C., Zhao, B., Kaneko, T. and Li, S. S.-C. (2012). Differential regulation of the activity of deleted in liver cancer 1 (DLC1) by tensins controls cell migration and transformation. *Proc. Natl. Acad. Sci. USA* **109**, 1455-1460.

Chaffer, C. L., San Juan, B. P., Lim, E. and Weinberg, R. A. (2016). EMT, cell plasticity and metastasis. *Cancer Metastasis Rev.* **35**, 645-654.

Cui, Y., Liao, Y. C. and Lo, S. H. (2004). Epidermal growth factor modulates tyrosine phosphorylation of a novel tensin family member, tensin3. *Mol. Cancer Res.* **2**, 225-232.

Defilippi, P., Di Stefano, P. and Cabodi, S. (2006). p130Cas: a versatile scaffold in signaling networks. *Trends Cell Biol.* **16**, 257-263.

Descot, A., Hoffmann, R., Shaposhnikov, D., Reschke, M., Ullrich, A. and Posern, G. (2009). Negative regulation of the EGFR-MAPK cascade by actin-MAL-mediated Mig6/Errfi-1 induction. *Mol. Cell* **35**, 291-304.

Duxbury, M. S., Ito, H., Zinner, M. J., Ashley, S. W. and Whang, E. E. (2004). CEACAM6 gene silencing impairs anoikis resistance and in vivo metastatic ability of pancreatic adenocarcinoma cells. *Oncogene* **23**, 465-473.

Frisch, S. M. and Francis, H. (1994). Disruption of epithelial cell-matrix interactions induces apoptosis. *J. Cell Biol.* **124**, 619-626.

Frisch, S. M. and Screaton, R. A. (2001). Anoikis mechanisms. *Curr. Opin. Cell Biol.* **13**, 555-562.

Geiger, B. and Yamada, K. M. (2011). Molecular architecture and function of matrix adhesions. *Cold Spring Harb. Perspect. Biol.* **3**, a005033.

Geiger, B., Bershadsky, A., Pankov, R. and Yamada, K. M. (2001). Transmembrane crosstalk between the extracellular matrix–cytoskeleton crosstalk. *Nat. Rev. Mol. Cell Biol.* **2**, 793-805.

Gilmore, A. P. (2005). Anoikis. *Cell Death Differ.* **12** Suppl. 2, 1473-1477.

Guadamillas, M. C., Cerezo, A. and Del Pozo, M. A. (2011). Overcoming anoikis–pathways to anchorage-independent growth in cancer. *J. Cell Sci.* **124**, 3189-3197.

Gunasinghe, N. P. A. P., Wells, A., Thompson, E. W. and Hugo, H. J. (2012). Mesenchymal-epithelial transition (MET) as a mechanism for metastatic colonisation in breast cancer. *Cancer Metastasis Rev.* **31**, 469-478.

Haynie, D. T. (2014). Molecular physiology of the tensin brotherhood of integrin adaptor proteins. *Proteins* **82**, 1113-1127.

Hofmann, C., Obermeier, F., Artinger, M., Hausmann, M., Falk, W., Schoelmerich, J., Rogler, G. and Grossmann, J. (2007). Cell-cell contacts prevent anoikis in primary human colonic epithelial cells. *Gastroenterology* **132**, 587-600.

Horton, E. R., Byron, A., Askari, J. A., Ng, D. H. J., Millon-Frémillon, A., Robertson, J., Koper, E. J., Paul, N. R., Warwood, S., Knight, D. et al. (2015). Definition of a consensus integrin adhesome and its dynamics during adhesion complex assembly and disassembly. *Nat. Cell Biol.* **17**, 1577-1587.

Humphries, M. J. and Reynolds, A. (2009). Cell-to-cell contact and extracellular matrix. *Curr. Opin. Cell Biol.* **21**, 613-615.

Kantak, S. S. and Kramer, R. H. (1998). E-cadherin regulates anchorage-independent growth and survival in oral squamous cell carcinoma cells. *J. Biol. Chem.* **273**, 16953-16961.

Katz, B.-Z., Zamir, E., Bershadsky, A., Kam, Z., Yamada, K. M. and Geiger, B. (2000). Physical state of the extracellular matrix regulates the structure and molecular composition of cell-matrix adhesions. *Mol. Biol. Cell* **11**, 1047-1060.

Katz, M., Amit, I., Citri, A., Shay, T., Carvalho, S., Lavi, S., Milanezi, F., Lyass, L., Amariglio, N., Jacob-Hirsch, J. et al. (2007). A reciprocal tensin-3-cten switch mediates EGF-driven mammary cell migration. *Nat. Cell Biol.* **9**, 961-969.

Lo, S. H. (2004). Tensin. *Int. J. Biochem. Cell Biol.* **36**, 31-34.

Lo, S. H. and Lo, T. B. (2002). Cten, a COOH-terminal tensin-like protein with prostate restricted expression, is down-regulated in prostate cancer. *Cancer Res.* **62**, 4217-4221.

Martuszewska, D., Ljungberg, B., Johansson, M., Landberg, G., Oslakovic, C., Dahlbäck, B. and Hafizi, S. (2009). Tensin3 is a negative regulator of cell migration and all four Tensin family members are downregulated in human kidney cancer. *PLoS ONE* **4**, e4350.

Mitra, S. K. and Schlaepfer, D. D. (2006). Integrin-regulated FAK-Src signaling in normal and cancer cells. *Curr. Opin. Cell Biol.* **18**, 516-523.

Ordonez, C., Screaton, R. A., Ilantzis, C. and Stanners, C. P. (2000). Human carcinoembryonic antigen functions as a general inhibitor of anoikis. *Cancer Res.* **60**, 3419-3424.

Paluch, E. K., Aspalter, I. M. and Sixt, M. (2016). Focal adhesion-independent cell migration. *Annu. Rev. Cell Dev. Biol.* **32**, 469-490.

Pankov, R., Cukierman, E., Katz, B.-Z., Matsumoto, K., Lin, D. C., Lin, S., Hahn, C. and Yamada, K. M. (2000). Integrin dynamics and matrix assembly: tensin-dependent translocation of alpha(5)beta(1) integrins promotes early fibronectin fibrillogenesis. *J. Cell Biol.* **148**, 1075-1090.

Paoli, P., Giannoni, E. and Chiarugi, P. (2013). Anoikis molecular pathways and its role in cancer progression. *Biochim. Biophys. Acta* **1833**, 3481-3498.

Qian, X., Li, G., Vass, W. C., Papageorge, A., Walker, R. C., Asnaghi, L., Steinbach, P. J., Tosato, G., Hunter, K. and Lowy, D. R. (2009). The Tensin-3 protein, including its SH2 domain, is phosphorylated by Src and contributes to tumorigenesis and metastasis. *Cancer Cell* **16**, 246-258.

Ramachandra, M., Atencio, I., Rahman, A., Vaillancourt, M., Zou, A., Avanzini, J., Wills, K., Bookstein, R. and Shabram, P. (2002). Restoration of transforming growth factor Beta signaling by functional expression of smad4 induces anoikis. *Cancer Res.* **62**, 6045-6051.

Schiller, H. B., Friedel, C. C., Boulegue, C. and Fässler, R. (2011). Quantitative proteomics of the integrin adhesome show a myosin II-dependent recruitment of LIM domain proteins. *EMBO Rep.* **12**, 259-266.

Shinchi, Y., Hieda, M., Nishioka, Y., Matsumoto, A., Yokoyama, Y., Kimura, H., Matsuura, S. and Matsuura, N. (2015). SUV420H2 suppresses breast cancer cell invasion through down regulation of the SH2 domain-containing focal adhesion protein tensin-3. *Exp. Cell Res.* **334**, 90-99.

Simpson, C. D., Anyiwe, K. and Schimmer, A. D. (2008). Anoikis resistance and tumor metastasis. *Cancer Lett.* **272**, 177-185.

Sun, Z., Guo, S. S. and Fässler, R. (2016). Integrin-mediated mechanotransduction. *J. Cell Biol.* **215**, 445-456.

Taddei, M. L., Giannoni, E., Fiaschi, T. and Chiarugi, P. (2012). Anoikis: an emerging hallmark in health and diseases. *J. Pathol.* **226**, 380-393.

Tang, X., Kuhlenschmidt, T. B., Zhou, J., Bell, P., Wang, F., Kuhlenschmidt, M. S. and Saif, T. A. (2010). Mechanical force affects expression of an in vitro metastasis-like phenotype in HCT-8 cells. *Biophys. J.* **99**, 2460-2469.

Tang, X., Kuhlenschmidt, T. B., Li, Q., Ali, S., Lezmi, S., Chen, H., Pires-Alves, M., Laegreid, W. W., Saif, T. A. and Kuhlenschmidt, M. S. (2014). A mechanically-induced colon cancer cell population shows increased metastatic potential. *Mol. Cancer* **13**, 131.

Touaitahuata, H., Morel, A., Urbach, S., Mateos-Langerak, J., de Rossi, S. and Blangy, A. (2016). Tensin 3 is a new partner of Dock5 that controls osteoclast podosome organization and activity. *J. Cell Sci.* **129**, 3449-3461.

Wulfaenger, J., Niedling, S., Riemann, D. and Seliger, B. (2008). Aminopeptidase N (APN)/CD13-dependent CXCR4 downregulation is associated with diminished cell migration, proliferation and invasion. *Mol. Membr. Biol.* **25**, 72-82.

Zaidel-Bar, R., Ballestrem, C., Kam, Z. and Geiger, B. (2003). Early molecular events in the assembly of matrix adhesions at the leading edge of migrating cells. *J. Cell Sci.* **116**, 4605-4613.

Zaidel-Bar, R., Cohen, M., Addadi, L. and Geiger, B. (2004). Hierarchical assembly of cell-matrix adhesion complexes. *Biochem. Soc. Trans.* **32**, 416-420.

Zamir, E. and Geiger, B. (2001). Molecular complexity and dynamics of cell-matrix adhesions. *J. Cell Sci.* **114**, 3583-3590.

Zamir, E., Katz, B. Z., Aota, S., Yamada, K. M., Geiger, B. and Kam, Z. (1999). Molecular diversity of cell-matrix adhesions. *J. Cell Sci.* **112**, 1655-1669.

Zamir, E., Katz, M., Posen, Y., Erez, N., Yamada, K. M., Katz, B.-Z., Lin, S., Lin, D. C., Bershadsky, A., Kam, Z. et al. (2000). Dynamics and segregation of cell-matrix adhesions in cultured fibroblasts. *Nat. Cell Biol.* **2**, 191-196.

Zhan, M., Zhao, H. and Han, Z. C. (2004). Signalling mechanisms of anoikis. *Histol. Histopathol.* **19**, 973-983.